ChemSusChem

Research Article
doi.org/10.1002/cssc.202200733

Chemistry Europe
European Chemical Societies Publishing

www.chemsuschem.org

Continuous Room-Temperature Hydrogen Release from Liquid Organic Carriers in a Photocatalytic Packed-Bed Flow Reactor

Malek Y. S. Ibrahim,[a] Jeffrey A. Bennett,[a] and Milad Abolhasani*[a]

Despite the potential of hydrogen (H_2) storage in liquid organic carriers to achieve carbon neutrality, the energy required for H_2 release and the cost of catalyst recycling have hindered its large-scale adoption. In response, a photo flow reactor packed with rhodium (Rh)/titania (TiO_2) photocatalyst was reported for the continuous and selective acceptorless dehydrogenation of 1,2,3,4-tetrahydroquinoline to H_2 gas and quinoline under visible light irradiation at room temperature. The tradeoff between the reactor pressure drop and its photocatalytic surface area was resolved by selective in-situ photodeposition of Rh in the photo flow reactor post-packing on the outer surface of the TiO_2 microparticles available to photon flux, thereby reducing the optimal Rh loading by 10 times compared to a batch reactor, while facilitating catalyst reuse and regeneration. An example of using quinoline as a hydrogen acceptor to lower the energy of the hydrogen production step was demonstrated via the water-gas shift reaction.

Introduction

Stringent regulations on carbon emissions are expected in the near future because of the accelerating negative environmental impacts of global warming.[1] Renewable energy sources including solar, wind, and biomass are attractive alternatives to fossil fuels that will help reduce worldwide carbon emissions. However, the intermittent nature of these alternative energy sources necessitates the development of green and sustainable energy storage and transportation technologies to maintain constant power supply. Hydrogen (H_2) is a clean and high-density form of energy storage that can be directly used in internal combustion engines and fuel cells.[2] The existing fuel storage and distribution infrastructure are designed to handle liquid fuels, and thus storing H_2 in the form of liquid organic hydrogen carrier (LOHC) allows for facile retrofitting of current global infrastructure for H_2 economy.[3]

Over the past decade, several catalytic processes have been developed for H_2 generation and storge.[4] However, the energy consumption and cost of generation and storage of H_2, including the water electrolysis ($>\$5\ kg^{-1}$), or the high temperature water-gas shift (WGS) reaction ($>400\,^{\circ}C$) as well as the cost of the H_2 storage/release process ($>\$1\ kg^{-1}$) hamper the overall feasibility of the process.[5] N-substituted heterocycles have lower dehydrogenation energy barrier when compared to cycloalkanes, and thus provide a low-energy opportunity for H_2 release.[6] Moreover, catalyst stability and recycling issues can further complicate the design of these processes.[7] Heterogeneous dehydrogenation catalysts that operate at temperatures higher than 120 °C and contain precious metal supported nanoparticles have been developed to address this issue at yields exceeding 95%. In one example, Deraedt et al. have shown that the dendrimer-stabilized nanoparticles of palladium (Pd), platinum (Pt), and rhodium (Rh) supported on SBA-15 silica can drive the dehydrogenation of 1,2,3,4-tetrahydroquinoline (THQ) to completion in 23 h at 130 °C.[8] In another study, Cui et al. have demonstrated that Pd_3Au_1 nanoparticles supported on carbon nanotubes could reduce the THQ dehydrogenation time by around 50% (12 h) at a slightly higher temperature (140 °C) and at a lower catalyst loading.[9] Non-precious metal catalysts have also been investigated to overcome the high cost of the precious metals. For example, it has been demonstrated that iron (Fe) could achieve dehydrogenation of THQ in 18 h at 145 °C, but at a lower yield (88%) than that obtained by precious metals,[10] while nitrogen assembly carbons can achieve >99% yield at 150 °C in 4 h or at room temperature in five days.[11]

From a sustainability perspective, a more energy-efficient acceptorless dehydrogenation process relies on the photo activation of the catalyst.[12] Metal-organic frameworks (MOFs) with narrow distance between their active sites have been shown to catalyze the dehydrogenation of THQ in 3 h under ultraviolet (UV) illumination (390 nm).[13] When the catalyst can be activated by visible light, the readily available solar irradiation can also be utilized to further increase the efficiency of the dehydrogenation process. Hexagonal boron carbon nitride (h-BCN) catalyst has been demonstrated to dehydrogenate THQ with blue light (420 nm) in 12 h at 79% yield.[14] In a recent study by Balayeva et al., THQ dehydrogenation yields up

[a] Dr. M. Y. S. Ibrahim, Dr. J. A. Bennett, Prof. M. Abolhasani
Department of Chemical and Biomolecular Engineering
North Carolina State University
911 Partners Way, Raleigh, NC 27695 (USA)
E-mail: abolhasani@ncsu.edu

Supporting information for this article is available on the WWW under https://doi.org/10.1002/cssc.202200733

to 99% have been achieved with Rh supported on anatase Hombikat titania (TiO_2) particles (≈1 μm particles) in 24 h with blue light (453 nm max.).[15] The ability to harvest visible light with TiO_2 is attributed to the ligand-to-metal charge transfer (LMCT) that occurs in the surface complex formed when the THQ amine coordinates to the surface of Ti^{4+} Lewis acid site. The Rh nanoparticles provide the metallic surface needed for recombinative desorption of H_2 in this case.

The thermo- and photocatalytic acceptorless dehydrogenation catalysts are conventionally tested in batch stirred reactors that require oxygen removal from the head space, generate catalyst fines, and require filtration/centrifugation for catalyst recycling, resulting in additional challenges when the process is scaled up. Moreover, batch reactors exhibit low surface area/volume ratio, which limits the ability to effectively harvest solar light. Microscale flow chemistry platforms with their high surface area/volume ratios have recently been demonstrated to successfully enable challenging chemical transformations, including homogeneous photocatalytic reactions.[16] However, heterogeneous photocatalytic microreactors are less common in literature, despite their potential to allow for the continuous and highly efficient photocatalytic H_2 release within a confined catalyst bed that exhibits high surface area/volume ratio, but also high pressure drop across the reactor.

In this study, we present a heterogeneous photocatalytic strategy using Rh/TiO_2 photocatalyst for highly efficient (>98% yield) continuous dehydrogenation of THQ at room temperature under low pressure drop (<60 psig; 1 psi = 6.89 kPa). We demonstrate that the optimal Rh loading in the photocatalytic flow reactor can be lowered from 1 to 0.025 wt% via an in-situ selective photodeposition of the precious metal in the flow reactor. Next, we study the long-term stability and regeneration of the developed dehydrogenation photocatalyst under continuous-flow conditions for more than 72 h. We also demonstrate the utility of quinoline as a H_2 acceptor in the low-temperature (<100 °C) H_2 transfer from water to quinoline under carbon monoxide (CO) using Rh catalyst and an auxiliary, short-chain tertiary amine.

The versatility of the flow chemistry strategy presented in this work, along with the ease of fabrication of the photocatalytic flow reactor, make it amenable to scale up and will have implications in energy storage and outer space manufacturing.

Results and Discussion

Heterogeneous photocatalytic dehydrogenation in flow

Inspired by the success of transparent flow reactors in homogeneous photocatalytic reactions, we opted to develop a flow chemistry strategy with a heterogeneous photocatalyst for room-temperature continuous dehydrogenation of THQ. Figure 1 presents the schematic of the developed flow chemistry platform for photocatalytic acceptorless dehydrogenation of THQ. The tubular photo flow reactor [fluorinated ethylene propylene (FEP); length: 25 cm, outer diameter: 1/8", inner diameter: 1/16"], fitted with polyetheretherketone (PEEK) frits, was packed with anatase TiO_2 microparticles (100–250 μm diameter) obtained from grinding and sieving commercially available pellets. It should be noted that to achieve sustainable dehydrogenation of THQ in the photo flow reactor using a heterogeneous catalyst, it is important to achieve low pressure drop (<10 psi cm^{-1}) across the reactor to reduce the input energy requirement (i.e., operational cost and carbon footprint) for flowing THQ through the reactor. When the flow reactor was packed with the Hombikat TiO_2 catalyst (≈1 μm diameter) reported in the batch process developed by Balayeva et al.,[17] the reactor fittings failed due to high pressure drop along the flow reactor (>100 psi.cm^{-1} at 50 mL.min^{-1} water flowrate). Following successful packing of the flow reactor with anatase TiO_2 microparticles (100–250 μm diameter), Rh was photodeposited on the surface of the packed anatase TiO_2 microparticles in situ. To achieve Rh loading on the packed TiO_2 microparticles, the void volume of the flow reactor was purged with argon and then filled with an argon-purged solution of Rh^{II} acetate dissolved in 1:2 (*v*/*v*) methanol(MeOH)/water(H_2O) under dark condition. The packed-bed photo flow reactor was then sealed and exposed to UV light (370 nm) for 3 h to allow for in-situ photodeposition of Rh on TiO_2. The photodeposition process (Figure S1) was repeated multiple times to approach the desired Rh loading (0.2 wt%). Following the photodeposition step, the packed-bed photo flow reactor was slowly vented to air and washed with water (50 mL min^{-1} for 8 h) before being dried in a static oven at 110 °C for 12 h. Following the drying step of one tube reactor, it was cooled to room temperature and purged with argon before testing for continuous dehydrogenation of THQ.

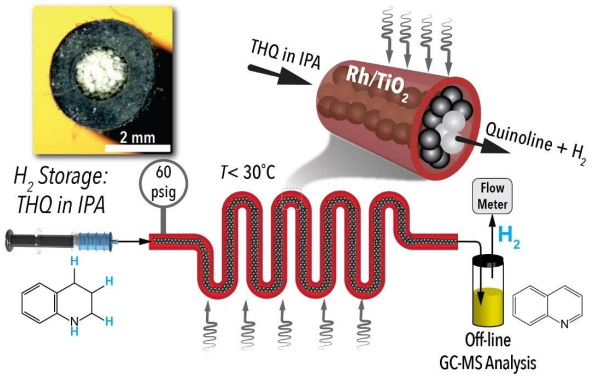

Figure 1. Schematic illustration of the photocatalytic tetrahydroquinoline dehydrogenation in a photo flow reactor packed with Rh/TiO_2 catalyst.

One packed-bed flow reactor was dedicated for photocatalyst characterization and cut open for catalyst sampling. Figure 2 presents a summary of the structural and optical characterizations of the in-situ photodeposited Rh/TiO_2 photo catalyst. The anatase TiO_2 crystals size was measured between 40 and 200 nm by transmission electron microscopy (TEM) images, shown in Figure 2A(i,ii). Energy-dispersive X-ray spectroscopy (EDS) mapping of the post-drying sample revealed Rh

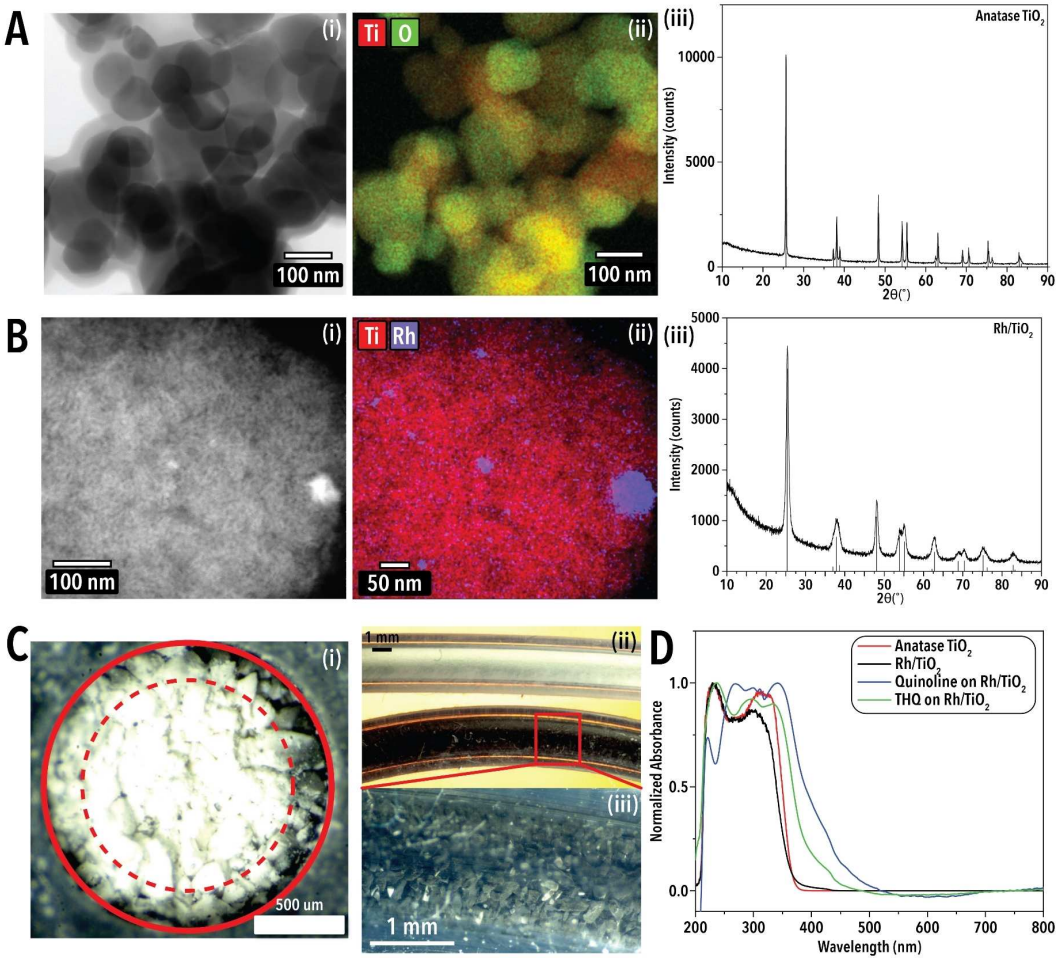

Figure 2. Characterization of Rh/TiO_2 photocatalyst synthesized via post-packing photodeposition in the photo flow reactor. Representative (i) TEM image, (ii) EDS map, and (iii) XRD pattern of the (A) pristine TiO_2 microparticles, and (B) Rh/TiO_2 microparticles adjacent to tube wall. (C) (i) Bright-field cross-sectional image of the packed-bed photo flow reactor after drying. (ii) Bright-field image of a packed-bed flow reactor with pristine TiO_2 microparticles (top) vs. Rh/TiO_2 microparticles (bottom). (D) UV/Vis absorption spectra of TiO_2 samples with Rh, THQ, and quinoline.

deposition in the form of scattered metallic nanoparticles in the range of 3–5 nm on the TiO_2 microparticles adjacent to the tube wall [Figure 2B (i,ii) and Figure S2]. X-ray diffraction (XRD) pattern of TiO_2 microparticles before and after deposition (Figure 2Aiii, Biii) illustrated peak broadening after deposition and drying, which can be attributed to generation of oxygen vacancies during the photodeposition process. The average Rh content on TiO_2 microparticles was measured by inductively coupled plasma mass spectrometry (ICP-MS). However, the cross-sectional images of the flow reactor, post-drying, revealed the formation of a dark region around the microparticles adjacent to the tube wall, while the microparticles closer to the center remained white, indicating a selective Rh deposition on TiO_2 microparticles around the tube wall (Figure 2C). The UV/Vis diffuse reflectance spectra of Rh/TiO_2 showed a slight adsorption edge over pristine anatase TiO_2 microparticles between 360 and 440 nm, which can be attributed to the plasmonic effect caused by Rh nanoparticles, Figure 2D. Adsorption of THQ and quinoline on TiO_2 illustrated a red shift in the UV/Vis absorption spectra with additional peaks at 335 and 343 nm, indicating the enhanced photon absorption in the visible light region by the surface complexes formed upon adsorption of the two molecules on the TiO_2 microparticles. Furthermore, the Rh photodeposition reduced the specific surface area of the microparticles from 172 to 46.7 $m^2 g^{-1}$ [measured using Brunauer-Emmett-Teller (BET) adsorption].

Following the structural and optical characterizations of the developed photocatalyst, we investigated its performance in photocatalytic acceptorless dehydrogenation of THQ. The solution of THQ in isopropanol (IPA) (0.1 M) was continuously fed to the packed-bed photo flow reactor under blue light illumination (427 nm), shown in Figure 1. The collected liquid effluents (Figure S3) under different reaction conditions were analyzed by gas chromatography-mass spectrometry (GC-MS). The gas effluent flow and composition were analyzed by a gas flow meter and gas chromatography-thermal conductivity detector (GC-TCD), respectively. At liquid flow rate of 3 $\mu L\,min^{-1}$, the quinoline yield was 7%, indicating slow kinetics at 0.2 wt% Rh/TiO_2. Following this observation, we studied the effect of Rh loading on the in-flow photocatalytic dehydrogenation of THQ

and found that the photocatalytic activity monotonically increased as the Rh precursor concentration was decreased, until maximum dehydrogenation yield was achieved at 0.025 wt% Rh/TiO_2 (Figure 3). The Rh loading lower than 0.025 wt% resulted in a decrease in quinoline yield, and in the absence of Rh, the quinoline yield was limited to only 5%. This behavior can be attributed to the slow H_2 desorption or proton reduction at the lower Rh loading and the decrease in photocatalytic activity by Rh nanoparticles at the higher loading. The optimal Rh loading is significantly lower in flow vs. batch reactor (0.5 to 1 wt%), mainly because of the selective Rh deposition on TiO_2 microparticles near the reactor walls, where the maximum photon flux is absorbed. As the photocatalytic dehydrogenation proceeds, gas bubbles are formed inside the reactor, which decrease the liquid residence time and the pressure drop (to 2 psi cm^{-1}; total 48 psig for a 25 cm-long reactor), and the estimated liquid residence time is 3 h.

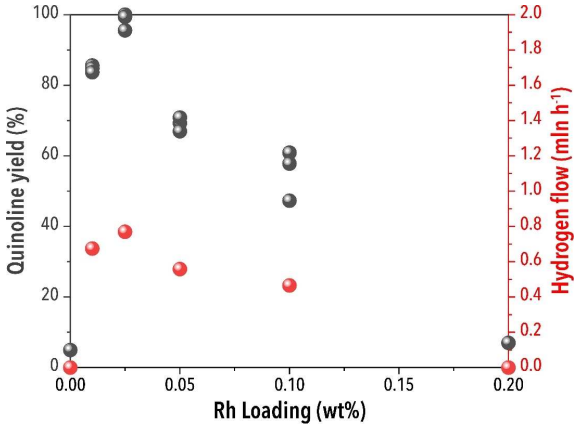

Figure 3. Quinoline yield and volumetric flowrate of the released H_2 from the continuous photocatalytic acceptorless THQ dehydrogenation process in the flow reactor under variable Rh loading (nominal Rh wt% on the TiO_2 particles after photoreduction). Photo flow reactor: FEP tubing with an outer diameter of 1/8", inner diameter of 1/16", and length of 25 cm. Liquid flowrate = 3 µL min^{-1} of 0.1 M THQ solution in IPA. Light source: 427 nm blue light at 55 mW cm^{-2} light intensity.

Complete dehydrogenation of THQ to quinoline was achieved when the Rh loading was 0.025 wt% and no other products were observed by GC-MS. At this Rh loading, the measured effluent gas flowrate was between 0.78 and 0.8 mL_n h^{-1}, equivalent to 97.0 to 99.5% of the stoichiometric H_2 flow at 100% quinoline yield. The H_2 flow rate decreased at Rh loadings higher and lower than the optimal 0.025 wt% loading, confirming the acceptorless dehydrogenation of the THQ across the conversion range studies here. The released H_2 flowrate was increased by increasing the THQ concentration at constant liquid flow rate and reactor length, while the quinoline yield was decreased (Figure 4A). This dichotomy can be explained by

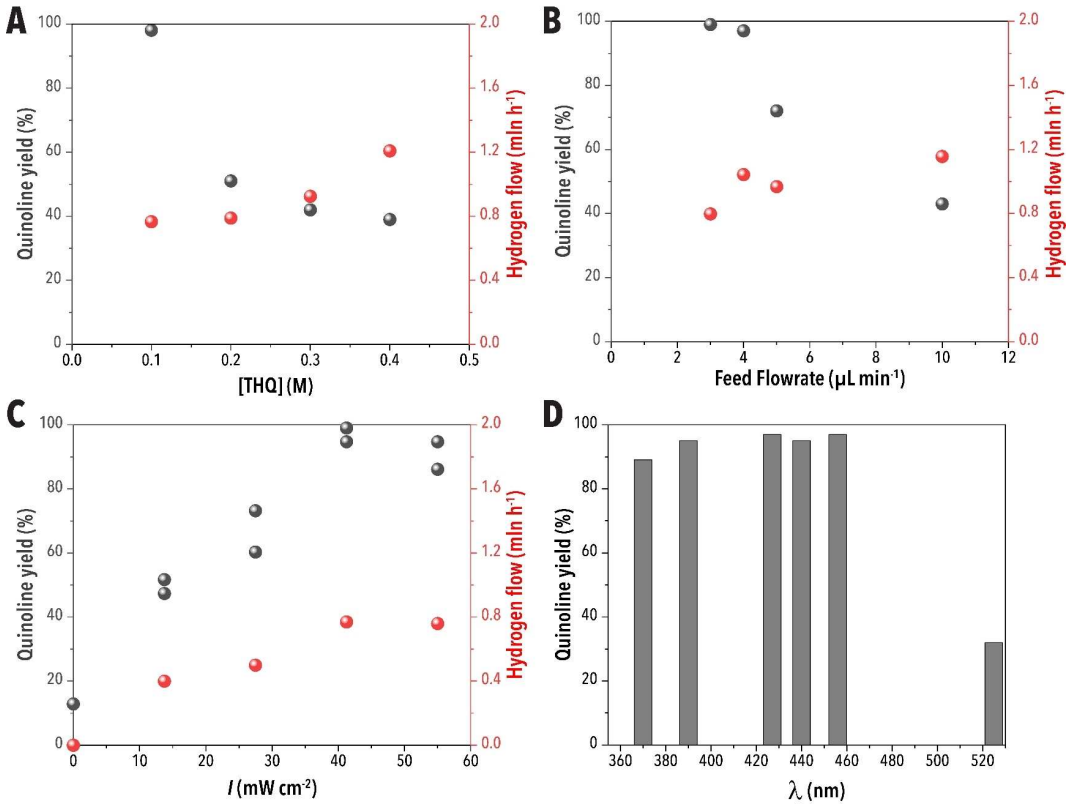

Figure 4. Effect of (A) THQ concentration, (B) feed flow rate, (C) light intensity, and (D) peak emission wavelength on the quinoline yield and released H_2 volumetric flowrate from the photo flow reactor packed with 0.025 wt% Rh/TiO_2 catalyst. Photo flow reactor: FEP tubing with an outer diameter of 1/8", inner diameter of 1/16", and length of 25 cm. Liquid flowrates in (A,C,D) = 3 µL min^{-1}. THQ concentration in (B–D) = 0.1 M in IPA. Light source peak emission wavelength in (A–C) = 427 nm. Light intensity was 55 mW cm^{-2}, unless otherwise mentioned in (C).

the decrease in the liquid residence time and thereby exposure to the effective photon flux in the packed-bed photo flow reactor, due to the formation of H_2 gas segments inside the reactor. When the

THQ concentration is doubled, the H_2 flowrate doubles for the same liquid feed flow rate at the same conversion, while the liquid residence time and quinoline yield decreased. At THQ concentration of 0.4 M, the quinoline yield decreased to 39% and the photocatalytically released H_2 flowrate increased to 1.2 $mL_n h^{-1}$ or 96% of the stoichiometric H_2 flow. It should be noted that the selectivity towards quinoline versus other products decreased from more than 97 to 88% and the pressure drop decreased from 2 to 1 psi cm^{-1} as the THQ concentration increased from 0.1 to 0.4 M.

Unlike THQ concentration, increasing the liquid flowrate from 3 to 4 μL min^{-1}, while maintaining the THQ concentration constant at 0.1 M did not result in a significant decrease in the quinoline yield, but increased the released H_2 flowrate to 1 $mL_n h^{-1}$ (Figure 4B). This can be attributed to the increase in pressure as the liquid velocity increases, and the formation of smaller H_2 gas bubbles at higher pressures. At liquid flow rates higher than 4 μL min^{-1}, the quinoline yield decreased to 43% at 10 μL min^{-1} and the H_2 flowrate reached 1.15 $mL_n h^{-1}$. At the THQ flowrate of 10 μL min^{-1}, the selectivity towards quinoline over other products remained higher than 97%, but the pressure drop increased to 10 psi cm^{-1}.

The geographical location and the weather conditions affect the intensity of the solar light, and thus the dehydrogenation efficiency of the packed-bed photo flow reactor. When the light intensity (I) was lowered to 75% of the maximum intensity of the utilized light source in this study (41 mW cm^{-2}), the quinoline yield and H_2 flowrate remained as high as 95% and 0.77 $mL_n h^{-1}$, respectively, indicating that the reaction was not limited by the photon flux at $I > 40$ mW cm^{-2} and 0.025 wt% Rh loading (Figure 4C). At light intensities below 40 mW cm^{-2}, the quinoline yield and the H_2 flowrate decreased monotonically until essentially no reaction occurred in the dark ($I = 0$). At maximum light intensity ($I = 55$ mW cm^{-2}), the quinoline yield remained higher than 95% when light sources with peak emission wavelengths (λ) of 390, 440, and 456 nm were used. However, a significant decrease of the quinoline yield down to 23% was observed when the light source peak emission wavelength was increased from 456 to 525 nm (Figure 4D).

The complete conversion per cycle and the rapid kinetics achieved with the developed photo flow reactor at room temperature brings the space-time yield (STY) for dehydrogenation up to 26.5 $g_{H_2} L^{-1} h^{-1}$ at a THQ concentration of 0.1 M. The STY is calculated using Equation (1):

$$\mathrm{STY} = \frac{n_A x_A M_A}{V_{Ao} t_R} \quad (1)$$

where n_A is the number of H_2 moles produced per mole of THQ, x_A is the equilibrium conversion, M_A is the molecular weight of H_2, V_{Ao} is the volume of one mole THQ in 0.1 M solvent, and t_R is the reaction time. The calculated STY of the developed photo flow reactor in this work is comparable to the STY obtained with thermal catalyst obtained at much higher temperatures for other carriers such as dibenzyltoluene (STY = 27.3 $g_{H_2} L^{-1} h^{-1}$ at 310 °C and methanol (STY = 44.2 $g_{H_2} L^{-1} h^{-1}$ at 420 °C).[18]

The average enthalpy of hydrogenation of quinoline to THQ is 62 kJ mol^{-1} H_2, which is considered a relatively high value for common liquid organic carriers. For example, the enthalpy of hydrogenation of *N*-ethylcarbazole is 53.2 kJ mol^{-1} H_2 and for formic acid is 31.2 kJ mol^{-1} H_2, while for methanol the value is only 16.5 kJ mol^{-1} H_2. The ability to drive the dehydrogenation of THQ with solar energy using the photo flow reactor, shown in Figure 1, makes the hydrogenation/dehydrogenation cycle energy negative. The surplus thermal energy generated in this cycle can be used for steam generation or heating. The elimination of the need to supply the heat of dehydrogenation brings the H_2 storage efficiency $\eta(H_2)$ for THQ from 65.6 to 79.5%. The $\eta(H_2)$ is calculated using Equation (2) reported by Niermann et al.:[18]

$$\eta(H_2) = \frac{E_{hyd} + E_{H2.use}}{E_{H2.in} + E_{storage} + E_{dhyd}} \quad (2)$$

where E_{hyd} and E_{dhyd} are the energy of hydrogenation and dehydrogenation, respectively, while $E_{H2.use}$ is the electricity generated in a fuel cell, and $E_{H2.in}$ is the energy required to generate H_2 via water electrolysis. The term $E_{storage}$ includes the energy required for blower and pumps, which are assumed to be the same for the thermal and photocatalytic dehydrogenation processes.

To elucidate the limiting step in the dehydrogenation reaction, the effect of oxidative vs. inert gas co-injection was studied on the photocatalytic activity and selectivity at 10 μL min^{-1} liquid flowrate. The quinoline yield decreased from 39 to 35.1% when argon was co-fed at 25 gas/liquid volumetric flow ratio (Table 1, entries 1 and 2). The decrease in the quinoline yield relative to the case when no gas was co-injected is attributed to the decreased liquid residence time. Replacement of the inert argon with air while keeping the reactor temperature below 30 °C allowed for complete conversion of the THQ, but the selectivity to quinoline was decreased to 85% (Table 1, entries 2 and 3). The increase in the quinoline conversion at the same light intensity in presence of air suggests that the acceptorless dehydrogenation process is limited by either proton reduction or recombinative desorption of H_2 to the gas phase and not the photocatalytic excitation at

Table 1. Photocatalytic acceptorless dehydrogenation of 1,2,3,4-THQ in flow. 0.025 wt% Rh/TiO_2 catalyst.[a]

Entry	T [°C]	Gas	1,2,3,4-THQ conv. [%]	Quinoline yield [%]
1	28	–	40.2	39.0
2	28	argon	35.7	35.1
3	28	air	99.9	85.5
4	65	argon	99.8	95.6

[a] Photo flow reactor: FEP tubing with an outer diameter of 1/8", inner diameter of 1/16", and length of 25 cm. Inlet liquid flowrate = 10 μL min^{-1}. THQ concentration = 0.1 M in IPA. Gas flow rate = 250 μL min^{-1}. Light source peak emission wavelength = 427 nm. Light intensity 55 mW cm^{-2}.

0.025 wt% Rh loading. Oxygen, on the other hand, reacts with the surface hydride species to form H_2O_2.[17] When the reaction temperature was increased to 65 °C, the conversion of THQ increased from 35.7 to 99.8% (Table 1, entries 2 and 4) indicating a high energy barrier for the reactor. However, thermal catalysis by Rh/TiO_2 is also possible in this case. Despite the rapid kinetics at 65 °C, the selectivity towards quinoline was less than 96%.

Benchmarking photocatalytic dehydrogenation in batch vs. flow reactors

Batch photocatalytic dehydrogenation reactions were performed to benchmark the performance of the optimized photo flow reactor (Figure S4). The liquid residence time inside the packed-bed photo flow reactor was calculated by measuring the difference in mass between the packed-bed reactor with/without segmented flow (i.e., gas-filled reactor vs. under reaction conditions) and was found to be 2.8 h. A 3 h photocatalytic dehydrogenation reaction in a batch reactor with a Rh loading similar to the optimized loading of the packed-bed photo flow reactor (0.025 wt%) resulted in a quinoline yield of only 11% (Table S2). Attempts to optimize the batch conditions by increasing the Rh loading or TiO_2 catalyst mass were not successful in increasing the quinoline yield higher than 25% in 3 h illumination time (Table S3). The results shown in Tables S2 and S3 confirm the superior performance of our developed packed-bed photo flow reactor for continuous energy-efficient photocatalytic dehydrogenation with a complete dehydrogenation in 3 h residence time in flow. The slower kinetics of the batch reactor compared to the photo flow reactor is attributable to the photo flux attenuation within 1 mm inside the batch reactor. Utilizing the TiO_2 fine powder (Hombikat, 1 μm diameter) instead of the anatase pellets in the batch reactor increased the quinoline yield to 29% in 3 h. However, this material is not a suitable candidate for packing flow reactors due to the significant increase in the pressure drop caused by the small particle size. Moreover, Rh deposition on a mixed-phase TiO_2 P25 (23% rutile, 77% anatase) was less effective as a dehydrogenation photocatalyst than the pure anatase pellets (Table S2), which is explained by the stronger contribution to surface reaction by charge carriers excited deeper in the bulk in anatase than rutile or mixed phase.[19]

Quinoline hydrogenation via WGS

The hydrogenation of quinoline to THQ with molecular hydrogen has been demonstrated to effectively proceed using supported metal nanoparticles, including Rh, Pd, Pt, and Pd alloys.[8,9,20] However, the energy needed for molecular H_2 production from water electrolysis or via the WGS reaction raises the cost of energy production/storage. Denmark et al. have recently demonstrated that the WGS can be carried out at room temperature with homogeneous Rh catalyst when activated methylene compounds are added as a hydride acceptor to turnover the catalyst.[21] Inspired by this result, we attempted the use of quinoline as a hydride acceptor to lower the temperature of the WGS and allow for the simultaneous H_2 transfer and storage in a single step from water.

In an earlier study by Murahashi et al., quinoline hydrogenation under WGS conditions was attempted, but the reaction was possible only at very high temperature (150 °C), very high CO pressure (800 psig), and high catalyst loading (4.8 mol% Rh), which made these conditions impractical for hydrogen storage.[22] At 80 °C and 350 pisg CO pressure, we observed no THQ formation after 15 h reaction time (Figure 5A). In the study by Denmark et al., it was demonstrated that the addition of a tertiary amine possessing short alkyl chain is essential to drive the hydrogenation of activated methylene compounds. The amine role in this case is to (1) raise the pH of the medium and maximize the concentration of the OH^- ions, and (2) ligate the Rh catalyst and suppress the catalyst aggregation in the presence of the CO ligand. When triethylamine (TEA) was added to the hydrogenation of quinoline under WGS at 0.125:1 amine/methanol (MeOH) volumetric ratio, the THQ yield increased from essentially 0 to 47% with 2 mol% Rh. Replacing TEA with *N*-methylpyrrolidine (MePryol), dimethylethylamine (DMEA), and *N*-methylpiperidine (MePip), increased the THQ yield to 55, 74, and 67%, respectively. Interestingly, when 1,2,2,6,6-pentamethylpiperidine (PMP) was applied as an auxiliary base to the WGS reaction, no THQ was formed, confirming the need for non-sterically hindered amines to drive the WGS reaction in presence of a hydride acceptor. Quinoline hydrogenation in solvents other than MeOH resulted in lower THQ yields (Figure 5B).

The optimal DMEA and water volumetric ratios relative to MeOH were found to be 0.125 and 0.5, respectively (Figure 5C,D). At lower amine or water volumetric ratios, the medium pH and the OH^- concentration are reduced, which results in slower H_2 transfer. The ability to significantly decrease the reaction temperature, pressure, and Rh loading upon the addition of the optimal amount of the auxiliary amine and water drastically lowers the energy required for H_2 production and storage from water. At 80 °C reaction temperature, the reaction can be conveniently driven by a solar thermal collector such as a parabolic trough.[23] Attempting to perform the WGS reaction in a segmented flow reactor by co-feeding the reaction liquid solution with CO gas (Figure S5) did not result in an increase in the reaction rate, indicating that the reaction is not limited by CO diffusion into the liquid phase at 350 psig (see Table S1). The ability to continuously generate stored H_2 in flow reactors allows for steady operation when considering H_2 storage-release cycle. However, solvent switch from methanol to isopropanol and the separation of the auxiliary amine are technological issues that need to be addressed when evaluating the feasibility of the hydrogen storage-release cycle.

Photocatalyst stability in the flow reactor

Following the development, optimization, and benchmarking of the packed-bed photo flow reactor, we investigated the long-

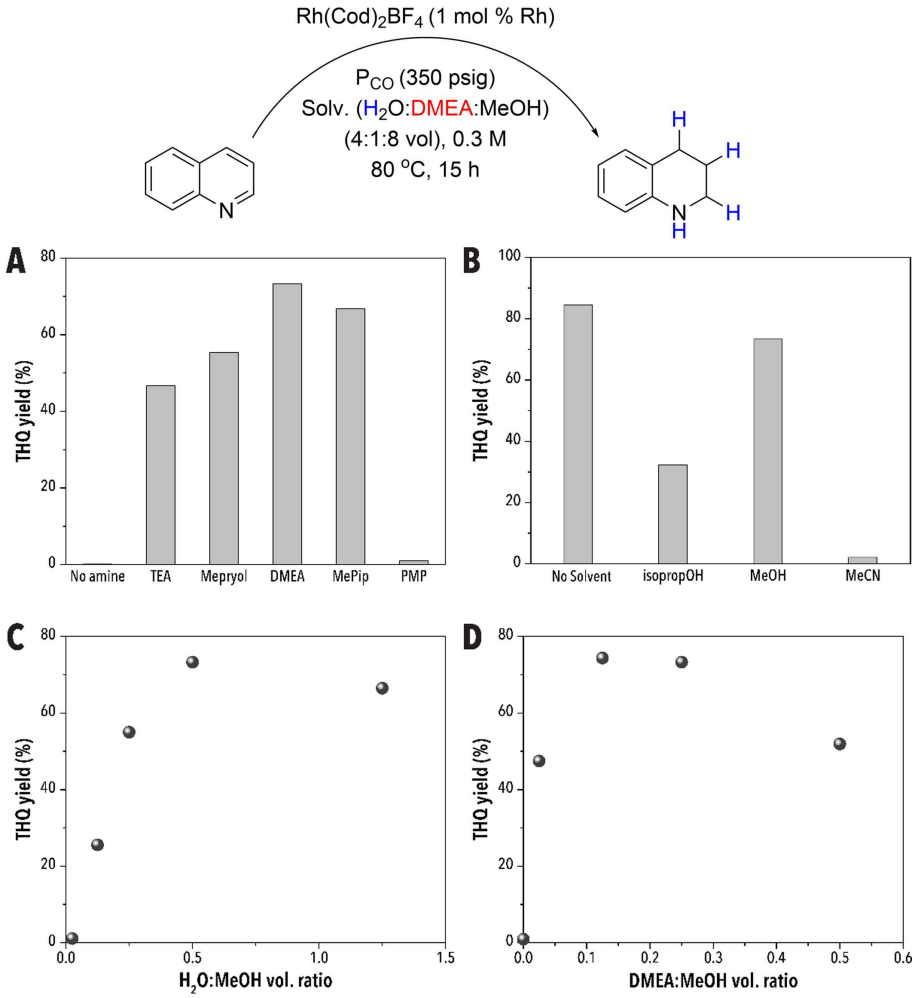

Figure 5. Effect of (A) auxiliary amine structure, (B) solvent, (C) dimethylamine volumetric ratio, and (D) water volumetric ratio on the THQ yield from 0.3 M quinoline hydrogenation under the WGS conditions in MeOH solvent at 80 °C, 350 psig CO pressure, and 1 mol% cyclooctadiene rhodium chloride dimer $[Rh(COD)Cl]_2$.

term stability of the heterogeneous photocatalyst over 72 h continuous operation using 0.1 M THQ in IPA. The quinoline yield and the released H_2 flowrate remained higher than 90% and 0.71 $mL_n h^{-1}$ for the first 60 h, respectively. Catalyst deactivation was observed beyond 60 h time on stream (TOS), and the quinoline yield and H_2 flowrate decreased to 78% and 0.61 $mL_n h^{-1}$ at TOS of 72 h (Figure 6A). The photocatalyst deactivation was accompanied by the formation of brown residue deposition on the dehydrogenation catalyst at the inlet side of the flow reactor (Figure 6B). The catalyst regeneration in the packed-bed photo flow reactor was performed in situ by flowing an air-water segmented flow under UV illumination (390 nm at $I = 55\ mW\,cm^{-2}$) for 6 h. MS analysis of the regeneration effluent showed the formation of the diamine. Under this regeneration condition, degradation and desorption of catalyst poisons, including diamines, occurred as indicated by the GC-MS analysis of the regeneration residue and the strong yellow color of the regeneration water effluent that changed to colorless as the catalyst regeneration proceeded (Figure 6C). The packed-bed flow reactor was then dried, purged with argon, and THQ dehydrogenation was continued for another 13 h during which the quinoline yield and H_2 flowrate rebound to 93% and 0.73 $mL_n h^{-1}$, respectively (Figure 6). To verify that the photocatalyst deactivation was not attributed to Rh leaching, the dehydrogenation liquid product was analyzed by ICP-MS and the Rh concentration was found to be 84.3 $\mu g\,L^{-1}$ or 0.36 $\mu g\ day^{-1}$ Rh loss rate under the testing liquid flow rate (i.e., 0.29% of the initial Rh mass is lost per day). Furthermore, the photocatalyst regeneration water effluent was also analyzed by ICP-MS and the Rh concentration was found to be 64.8 $\mu g\,L^{-1}$, indicating a minimal leaching under both the reaction and the regeneration conditions.

Conclusion

We demonstrated a sustainable and energy-efficient photocatalytic strategy for continuous and selective acceptorless dehydrogenation of 1,2,3,4-tetrahydroquinoline (THQ) in a transparent photo flow reactor packed with heterogeneous Rh/

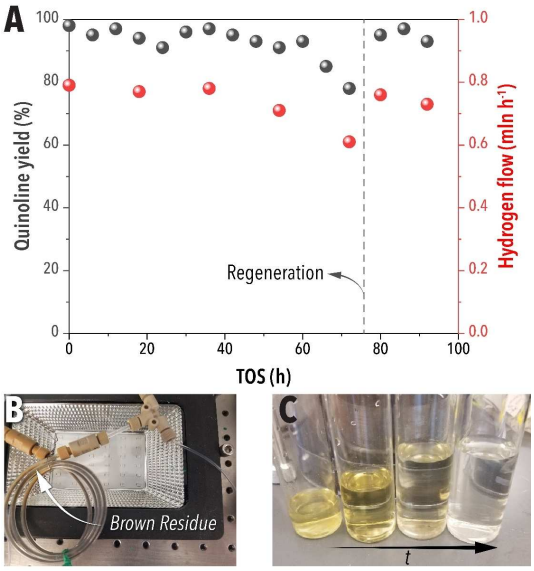

Figure 6. (A) Stability of the packed-bed photo flow reactor in terms of the quinoline yield and H_2 product volumetric flowrate using 0.025 wt% Rh/TiO_2 catalyst. Photo flow reactor: FEP tubing with an outer diameter of 1/8", inner diameter of 1/16", and length of 25 cm. Liquid flowrate = 3 μL min^{-1}. THQ concentration = 0.1 M in IPA. Light source peak emission wavelength = 427 nm blue light at 55 mW cm^{-2} intensity. (B) Formation of a brown residue on the dehydrogenation photocatalytic flow reactor on the inlet side after 60 h of operations. (C) Regeneration water effluent collected at different times from starting regeneration from left to right.

anatase TiO_2 catalyst. Post-packing Rh deposition on TiO_2 microparticles by UV photoreduction allowed for the selective Rh deposition in the fraction of the packed-bed reactor where photoexcitation occurs and lowered the optimal Rh loading to a fraction of what is needed when Rh photoreduction is carried out in a batch reactor. The developed packed-bed photo flow reactor allowed for on-site continuous production of high-purity H_2 gas. The released H_2 flow rate could be maximized by increasing the THQ concentration, or the liquid feed flowrate. The dehydrogenation activity increased with light intensity until it reached its maximum at 40 mW cm^{-2}. Moreover, an example of employing quinoline as a hydride acceptor to lower the energy cost of H_2 production was demonstrated by the water-gas shift reaction. Completing the energy-efficient cycle of quinoline hydrogenation/dehydrogenation using the developed acceptorless dehydrogenation strategy will allow for long-duration energy storage. The heterogeneous photo flow reactor reported in this study will find applications in a wide range of other photocatalytic reactions as well as outer space manufacturing.

Experimental Section

Photocatalytic THQ dehydrogenation in flow: A 25 cm Teflon tubing (FEP), inner diameter (ID): 1/16", outer diameter (OD): 1/8") was packed with TiO_2 ground pellets and fitted with 1 μm PEEK frits (reactor void volume ≈ 540 μL). The tube was purged with argon and the solution of Rh^{II} acetate was continuously fed to the packed-bed flow reactor using a syringe pump and then the reactor was exposed to UV LED. Next, deionized (DI) water was injected to wash the catalyst and then the reactor was dried in a drying oven (see the Supporting Information for details). A solution of THQ in anhydrous IPA was then continuously fed to the reactor at the desired liquid flow and the reactor was illuminated with a 427 nm LED at a light intensity of 60 mW cm^{-2}, unless otherwise mentioned. The reactor temperature was monitored with a thermocouple and maintained below 30 °C by flowing cold air between the coil and the LED from a Peltier cooler. As the dehydrogenation occurred in the flow reactor, gas bubbles were formed, which resulted in a gas-liquid segmented flow leaving the reactor. The effluent leaving the packed-bed photo flow reactor was directed to a sealed vial with a septum cap where gas-liquid separation was performed. The gas stream was routed through the septum to a bubble flow meter to measure the gas flowrate, while 100 μL samples were frequently taken from the collected liquid at the outlet for analysis by GC-MS.

Photodeposition and dehydrogenation in a batch reactor: The desired amount of the dried Rh/TiO_2 was weighed in an 8 mL glass vial and a stir bar was added. A solution of THQ in anhydrous IPA was prepared at the desired concentration (0.1 M) and added to the vial. The vial was then capped with a septum cap. The slurry solution was purged with argon for 1 h and the sealed vial was placed on a stir plate (800 rpm) and illuminated by a 427 nm LED at a light intensity of 60 mW cm^{-2}. The vial temperature was monitored with a thermocouple and maintained below 30 °C by flowing cold air between the reactor and the LED from a Peltier cooler. An aluminum foil layer was placed on the non-illuminated side of the glass vial to maximize light absorption by the photocatalyst from all sides. The reaction was run for 24 h. An aliquot was then then filtered through a celite bed and analyzed by GC-MS.

Effluent analysis during the regeneration of the packed-bed flow reactor: A segmented flow of DI water/air was fed to the bed at 50 μL min^{-1} and 0.2 mL_n min^{-1}, respectively, using a syringe pump (HARVARD PHD ULTRA) and a mass flow controller (EL-Flow®, Bronkhorst). The packed-bed photo flow reactor was illuminated by UV LED (390 nm at I = 55 mW cm^{-2}) for 6 h, while the segmented flow was moving through the reactor to affect catalyst poisons degradation and desperation. The initial fraction of the effluent water was pumped down under vacuum and the residue was analyzed by GC-MS. The detected mass was 262 *m/z*, indicating the formation of diamine products that can potentially bind strongly on the surface and inhibit the reaction.

Hydrogenation of quinoline under WGS condition in a segmented flow reactor: An 8 mL stainless-steel syringe connected to a Teflon tubing (FEP, OD: 1/16", ID: 0.01") was filled with the reaction solution containing the catalyst, solvent, water, amine, and quinoline, and the liquid was fed to the reactor coil using a syringe pump. Gas-liquid segmentation was achieved by contacting the liquid stream with the CO gas flow in a stainless-steel T-junction (1/8" OD, Swagelok) before entering the stainless-steel flow reactor (OD:1/8", ID:1/16", and 94 cm length); gas flowrate was controlled by a mass flow controller (EL-Flow®, Bronkhorst). The segmented flow reactor temperature was controlled using a hotplate and oil bath with a temperature probe immersed in the oil bath. The flow reactor pressure was controlled with a backpressure regulator (Equilibar) integrated at the outlet of the flow reactor. Product analysis was performed by GC-MS.

Hydrogenation of quinoline under WGS condition in a batch reactor: The reaction was performed in a Buchi Tinyclave pressure vessel. A solution of cyclooctadiene rhodium chloride dimer $[Rh(COD)Cl]_2$ was prepared in anhydrous methanol and added to a 4 mL glass vial with a stir bar. The DI water, amine, and quinoline were added to the vial. The vial was transferred to the pressure

vessel and pressurized to the desired pressure (350 psig unless otherwise mentioned), then placed on a hot stir plate (80 °C, 800 rpm). The hydrogenation reaction was conducted for 15 h. The pressure vessel was then cooled down, vented, and purged with N_2 before opening. An aliquot was taken from the organic layer for analysis by GC-MS.

Acknowledgements

The authors gratefully acknowledge the financial support from North Carolina State University. This work was performed in part by the Molecular Education, Technology, and Research Innovation Center (METRIC) at North Carolina State University, which is supported by the State of North Carolina. This work was performed in part by the Analytical Instrumentation Facility (AIF) at North Carolina State University, which is supported by the State of North Carolina. The authors thank Venator for providing Hombikat UV-100 sample for testing.

Conflict of Interest

The authors have filed a US Provisional Patent Application, U.S. patent 63/323,214, based on the results of this work. The authors declare no other competing interests.

Data Availability Statement

The data that support the findings of this study are available from the corresponding authors upon request.

Keywords: dehydrogenation · flow chemistry · hydrogen storage · photo flow reactor · photocatalysis

[1] S. M. S. U. Eskander, S. Fankhauser, *Nat. Clim. Change* **2020**, *10*, 750–756.
[2] S. van Renssen, *Nat. Clim. Change* **2020**, *10*, 799–801.
[3] a) R. H. Crabtree, *Energy Environ. Sci.* **2008**, *1*, 134–138; b) Q.-L. Zhu, Q. Xu, *Energy Environ. Sci.* **2015**, *8*, 478–512.
[4] a) J. Kothandaraman, S. Kar, R. Sen, A. Goeppert, G. A. Olah, G. K. S. Prakash, *J. Am. Chem. Soc.* **2017**, *139*, 2549–2552; b) M. Navlani-García, K. Mori, Y. Kuwahara, H. Yamashita, *NPG Asia Mater.* **2018**, *10*, 277–292; c) S. Dutta, *J. Ind. Eng. Chem.* **2014**, *20*, 1148–1156.
[5] C. Weidenthaler, M. Felderhoff, *Energy Environ. Sci.* **2011**, *4*, 2495–2502.
[6] A. Moores, M. Poyatos, Y. Luo, R. H. Crabtree, *New J. Chem.* **2006**, *30*, 1675–1678.
[7] K. C. Tan, T. He, Y. S. Chua, P. Chen, *J. Phys. Chem. C* **2021**, *125*, 18553–18566.
[8] C. Deraedt, R. Ye, W. T. Ralston, F. D. Toste, G. A. Somorjai, *J. Am. Chem. Soc.* **2017**, *139*, 18084–18092.
[9] X. Cui, Z. Huang, A. P. V. Muyden, Z. Fei, T. Wang, P. J. Dyson, *Sci. Adv.* **2020**, *6*, eabb3831.
[10] G. Jaiswal, V. G. Landge, D. Jagadeesan, E. Balaraman, *Nat. Commun.* **2017**, *8*, 2147.
[11] H. Hu, Y. Nie, Y. Tao, W. Huang, L. Qi, R. Nie, *Sci. Adv.* **2022**, *8*, eabl9478.
[12] Q. Wang, C. Pornrungroj, S. Linley, E. Reisner, *Nat. Energy* **2022**, *7*, 13–24.
[13] X. Gong, Y. Shu, Z. Jiang, L. Lu, X. Xu, C. Wang, H. Deng, *Angew. Chem. Int. Ed.* **2020**, *59*, 5326–5331.
[14] M. Zheng, J. Shi, T. Yuan, X. Wang, *Angew. Chem. Int. Ed.* **2018**, *57*, 5487–5491.
[15] N. O. Balayeva, Z. Mamiyev, R. Dillert, N. Zheng, D. W. Bahnemann, *ACS Catal.* **2020**, *10*, 5542–5553.
[16] a) L. Buglioni, F. Raymenants, A. Slattery, S. D. A. Zondag, T. Noël, *Chem. Rev.* **2021**; b) C. Sambiagio, T. Noël, *Trends Chem.* **2020**, *2*, 92–106.
[17] N. O. Balayeva, N. Zheng, R. Dillert, D. W. Bahnemann, *ACS Catal.* **2019**, *9*, 10694–10704.
[18] M. Niermann, S. Drünert, M. Kaltschmitt, K. Bonhoff, *Energy Environ. Sci.* **2019**, *12*, 290–307.
[19] T. Luttrell, S. Halpegamage, J. Tao, A. Kramer, E. Sutter, M. Batzill, *Sci. Rep.* **2014**, *4*, 4043.
[20] a) R. A. Sánchez-Delgado, N. Machalaba, N. Ng-a-qui, *Catal. Commun.* **2007**, *8*, 2115–2118; b) J. Zhao, H. Yuan, G. Yang, Y. Liu, X. Qin, Z. Chen, C. Weng-Chon, L. Zhou, S. Fang, *Nano Res.* **2022**, *15*, 1796–1802.
[21] S. E. Denmark, M. Y. S. Ibrahim, A. Ambrosi, *ACS Catal.* **2017**, *7*, 613–630.
[22] S. Murahashi, Y. Imada, Y. Hirai, *Bull. Chem. Soc. Jpn.* **1989**, *62*, 2968–2976.
[23] L. A. Weinstein, J. Loomis, B. Bhatia, D. M. Bierman, E. N. Wang, G. Chen, *Chem. Rev.* **2015**, *115*, 12797–12838.

Manuscript received: April 11, 2022
Revised manuscript received: April 20, 2022
Accepted manuscript online: April 21, 2022
Version of record online: May 18, 2022